Mon. Not. R. Astron. Soc. **000**, 1–14 (200X) Printed 24 May 2010 (MN LaTeX style file v2.2)

arXiv:1005.3649v2 [astro-ph.CO] 21 May 2010

Wide-angle tail galaxies in ATLAS

Minnie Y. Mao[1,2,3⋆], Rob Sharp[2], D. J. Saikia[3,4,5], Ray P. Norris[3],
Melanie Johnston-Hollitt[6], Enno Middelberg[7] and Jim E. J. Lovell[1]
[1] *School of Mathematics and Physics, University of Tasmania, Private Bag 37, Hobart, 7001, Australia*
[2] *Anglo-Australian Observatory, PO Box 296, Epping, NSW, 1710, Australia*
[3] *CSIRO Australia Telescope National Facility, PO Box 76, Epping, NSW, 1710, Australia*
[4] *National Centre for Radio Astrophysics, Tata Insitute of Fundamental Research, Pune 411 007, India*
[5] *ICRAR, University of Western Australia, Crawley, WA 6009, Australia*
[6] *School of Chemical and Physical Sciences, Victoria University of Wellington, PO Box 600, Wellington, New Zealand*
[7] *Astronomisches Institut, Ruhr-Universität Bochum, Universitätsstr. 150, 44801 Bochum, Germany*

200X

ABSTRACT

We present radio images of a sample of six Wide-Angle Tail (WAT) radio sources identified in the ATLAS 1.4 GHz radio survey, and new spectroscopic redshifts for four of these sources. These WATs are in the redshift range of $0.1469-0.3762$, and we find evidence of galaxy overdensities in the vicinity of four of the WATs from either spectroscopic or photometric redshifts. We also present follow-up spectroscopic observations of the area surrounding the largest WAT, S1189, which is at a redshift of $\sim$0.22. The spectroscopic observations, taken using the AAOmega spectrograph on the AAT, show an overdensity of galaxies at this redshift. The galaxies are spread over an unusually large area of $\sim$12 Mpc with a velocity spread of $\sim$4500 km s^{-1}. This large-scale structure includes a highly asymmetric FRI radio galaxy and also appears to host a radio relic. It may represent an unrelaxed system with different sub-structures interacting or merging with one another. We discuss the implications of these observations for future large-scale radio surveys.

Key words: galaxies: clusters: general – galaxies: active – galaxies: general – radio continuum: galaxies – galaxies: distances and redshifts

1 INTRODUCTION

Wide-Angle Tail (WAT) galaxies are radio galaxies whose radio jets appear to bend in a common direction. They are generally detected in dynamical, non-relaxed clusters of galaxies (e.g. Burns 1990) and may be used as probes or tracers for clusters (Blanton et al. 2000, 2001). Clusters of galaxies are the largest gravitationally bound structures in the Universe and are powerful testbeds of cosmological models (e.g. Borgani et al. 2004; Sahlén et al. 2009; Kravtsov et al. 2009). Clusters also host diffuse radio emission in the form of radio haloes and relics (Giovannini & Feretti 2000; Feretti 2005; Ferrari et al. 2008; Giovannini et al. 2009).

The bent nature of WATs has commonly been attributed to strong intra-cluster winds caused by dynamical interactions such as cluster-cluster mergers (Burns 1998). WATs are preferentially found in enhanced X-ray regions (Pinkney et al. 2000) and are usually associated with dominant cluster galaxies (Owen & Rudnick 1976). Mao et al. (2009a) found the tailed radio galaxies, including WATs, to be located in the densest regions of clusters in the local Universe, consistent with earlier studies (e.g. Burns 1990; Blanton et al. 2000, 2001). Thus WATs represent valuable tracers of high density regions in the intracluster medium (ICM), and this approach has been used in a number of recent studies (e.g. Blanton et al. 2000, 2003; Smolcić et al. 2006; Giacintucci & Venturi 2009; Kantharia, Das & Gopal-Krishna 2009; Oklopcic et al. 2010).

Here we present the radio properties of six WATs

⋆ e-mail: mymao@utas.edu.au

© 200X RAS

that we have identified in ATLAS, the Australia Telescope Large Area Survey, carried out with the Australia Telescope Compact Array (ATCA) at 1.4 GHz (Norris et al. 2006; Middelberg et al. 2008). ATLAS [1] will image seven square degrees of sky over two fields to an rms sensitivity of 10 μJy beam^{-1}. The ATLAS fields have been observed with a number of different ATCA configurations, and the typical resolution of the observations is ∼10 arcsec. The two ATLAS fields, Chandra Deep Field South (CDFS) and European Large Area ISO Survey-South 1 (ELAIS-S1), were chosen to coincide with the *Spitzer* Wide-Area InfraRed Extragalactic (SWIRE) survey program (Lonsdale et al. 2003) so that corresponding optical and infrared photometric data are available.

In addition to the radio properties we present new spectroscopic redshifts for four of the WATs and follow-up spectroscopic observations of galaxies in the vicinity of the largest WAT in order to probe its surrounding structure. This WAT was first identified as radio source S1189 by Middelberg et al. (2008), and is associated with the SWIRE source SWIRE4_J003427.54-430222.5 (Lonsdale et al. 2003).

In this paper we present a summary of the data in Section 2, while the WATs in ATLAS are presented in Section 3. Section 4 presents the results of spectroscopic observations of S1189 and its surrounding region, and discusses the large-scale structure in its vicinity. In Section 5 we discuss cosmological inverse-Compton quenching and the implications for deep wide radio surveys and ATLAS. This paper uses $H_0 = 71$ km s^{-1} Mpc^{-1}, $\Omega_M = 0.27$ and $\Omega_\Lambda = 0.73$ and the web-based calculator of Wright (2006) to estimate the physical parameters. Vega magnitudes are used throughout.

2 DATA

2.1 Radio Data

ATLAS radio observations are currently partially complete with an rms noise of ∼20 - 30 μJy beam^{-1} at 1.4 GHz. The data used in this paper are taken from the first ATLAS catalogues (Norris et al. 2006; Middelberg et al. 2008) which contain 2004 radio sources. We expect ∼16000 radio sources at the completion of the survey.

2.2 Spectroscopy

As part of ATLAS, we are undertaking a program of redshift determination and source classification of all ATLAS radio sources with AAOmega (Sharp et al. 2006) on the Anglo-Australian Telescope (AAT). We are currently partway through our ATLAS spectroscopy campaign. A summary of these observations are presented by Mao et al. (2009b) while the detailed results will be presented by Mao et al. (in preparation). 169 ATLAS sources already have spectroscopic redshifts from the literature. We have obtained 395 new spectroscopic redshifts using AAOmega giving a total so far of 564 spectroscopic redshifts: 261 in CDFS and 303 in ELAIS-S1. All of the WATs presented in this paper have spectroscopic data from either our AAT observations or 2dFGRS (Colless et al. 2001).

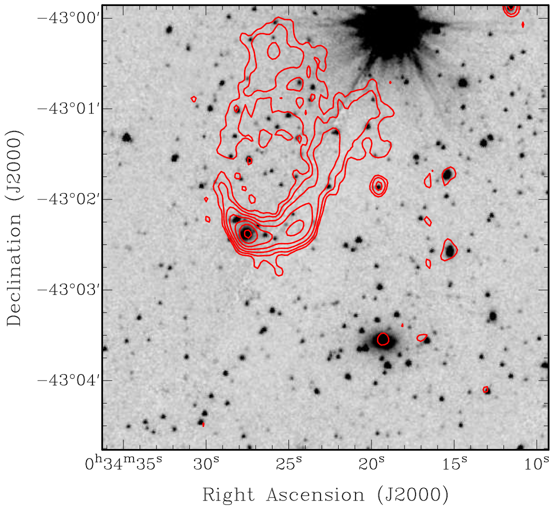

Figure 1. SWIRE 3.6-μm image of the WAT, S1189, and the putative cD galaxy located south-west of the WAT. The 1.4 GHz radio contours which are overlaid start from 100 μJy beam^{-1} (3 × rms) and increase by factors of 2.

2.3 Follow-up Spectroscopy of the region around S1189

There appears to be a cluster of galaxies within ∼2 arcmin of S1189 in the optical and infrared images (see Fig. 1). We obtained AAOmega observations for sources within a degree of S1189 in service mode during the night of 2008 October 18. The AAOmega spectrograph was used in multi-object mode (Saunders et al. 2004; Sharp et al. 2006) and centred on the WAT. We used the dual beam system with the 580V and 385R Volume Phase Holographic (VPH) gratings centred at λ4800 and λ7150 covering the spectral range between 3700Å and 8500Å at central resolutions in each arm of R∼1300 per 3.4 pixel spectral resolution element. The 5700Å dichroic beam splitter was used. Observing conditions were good with clear skies and an average seeing of ∼1.6 arcsec. Two fibre configurations were observed with 3 × 1200 sec integrations and associated quartz-halogen flat fields and combined CuAr+FeAr, Helium and Neon arc lamp frames.

Targets were identified from the SWIRE catalogues (Lonsdale et al. 2003). The target magnitude range was limited to $19 < R < 20.5$. The bright limit was chosen to select against foreground galaxies based on the expected low number of galaxies brighter than L* in the potential cluster. The faint limit was chosen due to the bright-of-moon service observations. The magnitude range yielded ∼7000 sources within a one degree radius (the field of view of the

---

[1] http://www.atnf.csiro.au/research/deep/index.html

2dF/AAOmega fibre positioner (Lewis et al. 2002)) centered on S1189[2]. Targets were prioritized based on radial separation from the WAT S1189 with the exception of the putative cD galaxy which was assigned the highest priority to ensure that its redshift was obtained. Targets farther than 5 arcmin were randomly sampled using Fisher-Yates shuffles, to decrease the input catalogue to a practical working sample for the CONFIGURE software and the Simulated Annealing fibre allocation algorithm (Miszalski et al. 2006), as given in Table 1. Regrettably no star-galaxy separation was performed resulting in the inclusion of stars in the input catalogue. Although ∼400 AAOmega science fibres are available, fibre allocation requires target separations in excess of 30 arcsec due to physical limitations. Consequently two independent fibre configurations were observed to secure as many high priority sources as possible.

Data reduction followed the standard pattern for AAOmega spectroscopy using the `2dfdr` software package. The red and blue arms were reduced independently and then spliced together so as to produce a continuous spectrum. The redshift was then determined from the spectra using `runz`.

3 WATS IN ATLAS

We have identified six WATs in ATLAS by visually examining the greyscale ATLAS images (Norris et al. 2006; Middelberg et al. 2008). Fig. 2 shows the ATLAS greyscale radio images of the WATs in the left column, while images of the WATs superposed on the Digitized Sky Survey (DSS) red and 3.6-μm Infrared Array Camera (IRAC) images are shown in the middle and right columns respectively. The WATs range in redshift from 0.1469 to 0.3762, and their properties are summarized in Table 2. The radio luminosities at 1.4 GHz range from $\sim 2-6 \times 10^{24}$ W Hz^{-1} which places them in the FRI (Fanaroff & Riley 1974) category. For comparison the median luminosities of radio sources associated with cD galaxies in rich and poor clusters studied by Giacintucci et al. (2007) are 0.7×10^{24} and 0.2×10^{24} W Hz^{-1} at 1.4 GHz. We have estimated the absolute R-band magnitudes of our ATLAS sources and find that these lie close to the transition region in the absolute red-magnitude−1.4 GHz radio luminosity plot of Owen & Ledlow (1994). The optical spectra of the five sources for which we have determined redshifts, of which four (S132, S483, S1189 and S1192) are new, are presented in Fig. 3. The redshift of the sixth WAT galaxy, S409, was determined by Colless et al. (2001).

We have probed for overdensities of galaxies in the vicinity of the WATs. In addition to our observations of S1189 mentioned earlier, we have examined the 2dFGRS (Colless et al. 2001) spectroscopic survey, as well as the photometric redshifts of galaxies in the *SWIRE* field by Rowan-Robinson et al. (2008). The 2dFGRS shows an overdensity of galaxies associated with S409, which is the nearest WAT in our sample, while the photometric redshifts indicate overdensities of galaxies associated with S483 and S1192.

We have examined archival *ROSAT* All-Sky Survey (RASS) data for X-ray detections, and found no RASS detections towards these WATs. This implies an upper limit to the X-ray luminosity of potential host clusters of $\sim 2-11 \times 10^{37}$ W s^{-1} which spans the upper values typical for clusters of galaxies with known X-ray emission (Böhringer et al. 2001). This indicates upper limits to the masses of $\sim 2-6 \times 10^{14} \mathrm{M}_{\odot}$ (Pratt et al. 2009).

3.1 S132

The largest angular size of the source from end to end along the axis of the source is 0.96 arcmin, corresponding to a physical size of ∼309 kpc. The peak of emission to the southwest of the host galaxy has been determined to be an unrelated source, S131 (Middelberg et al. 2008). There are several galaxies to the west of the southern tail which are seen more clearly in the 3.6-μm image, but at present no redshift information is available for these galaxies. The tails appear to bend away from this overdensity of galaxies.

3.2 S483

This WAT, which has an overall linear size of 413 kpc, is highly asymmetric in the brightness of the two tails, with the peak brightness in the northern tail being higher by a factor of ∼5. It would be useful to image the source, especially the southern tail, with higher surface brightness sensitivity to confirm the present classification. The photometric redshifts of the galaxies (Rowan-Robinson et al. 2008) within a radius of 2 arcmin, which corresponds to ∼550 kpc at z=0.3164, show a concentration of galaxies at about the redshift of S483 (Fig. 4).

3.3 S1189

S1189 is the largest WAT in our sample with an overall linear size of ∼1053 kpc. Its opening angle, defined by the lines connecting the regions of highest surface brightness to the optical galaxy is ∼70°, which is slightly smaller than for the high-redshift WAT reported by Blanton et al. (2001) which has an opening angle of ∼80°. Clearly these opening angles would depend on the resolution of the observations and projection effects. Rudnick & Owen (1977) distinguish between narrow-, intermediate- and wide-angle tails by requiring that the opening angle be less than ∼20° for narrow-angle tailed sources and greater than ∼90° for WATs, based largely on tailed sources at smaller redshifts than our sources. Although it would be relevant to examine the effects of resolution and surface brightness sensitivity as one

---

[2] The SWIRE input catalogue of Lonsdale et al. (2003) excludes a number of small regions at the outer edge of the field.

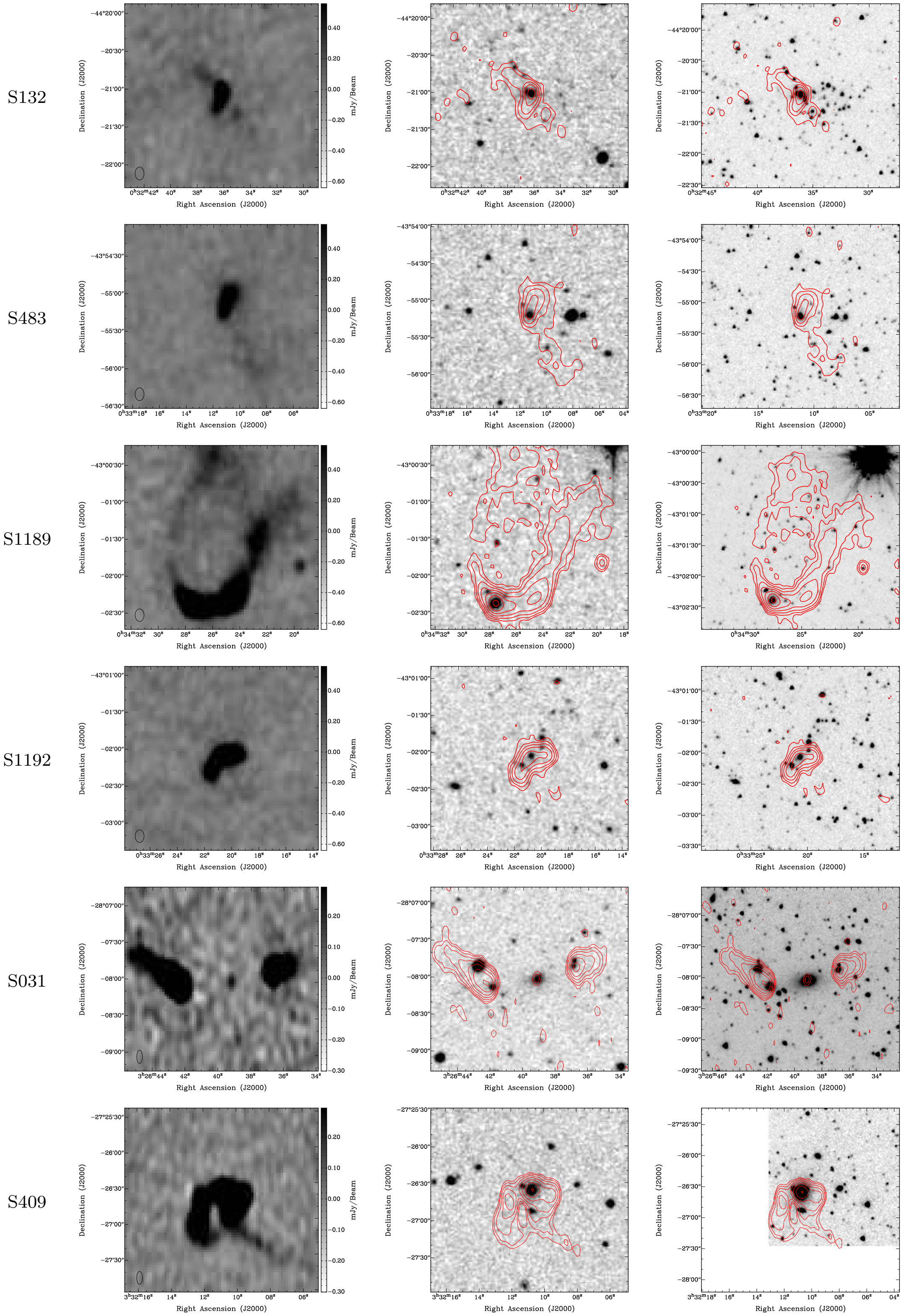

Figure 2. The six WATs in ATLAS. From top to bottom the WATs are S132, S483, S1189 and S1192 in ELAIS-S1, and S031 and S409 in CDFS. The left column shows the 1.4 GHz radio continuum emission of the WATs in greyscale.The middle column shows the radio contours overlaid on DSS red images. The right column shows the radio contours overlaid on 3.6-μm IRAC images. The radio contours start from 100 μJy beam $^{-1}$(3 × rms) and increase by factors of 2. S409 is located at the edge of the 3.6-μm image.

Table 1. Priority assignment for the target observations. AAOmega is configured based on source location and user-defined priority assignment with 9 being the highest priority and 1 being the lowest. Columns 1 and 2 list the priority assignment and the number of sources in each priority bin. Column 3 presents the number of sources for which we were able to obtain redshifts, while Column 4 gives the radii of the priority bin from S1189. Column 5 describes how many sources were selected randomly using Fisher-Yates shuffles. Priority 1 sources were not included in the target list.

Priority	No. sources	Redshifts	Radii	Comment
9	1	1		putative cD
8	12	0	$< 2'$	
7	60	7	$2'$ to $5'$	
6	100	8	$5'$ to $10'$	100/187 randomly selected
5	200	15	$10'$ to $15'$	200/328 randomly selected
4	200	28	$1'5$ to $30'$	200/1956 randomly selected
3	200	19	$30'$ to 1 deg	200/4426 randomly selected
2	46	8		sources with previously determined z_{spec}
1	6197	0	$> 5'$	sources not randomly selected

Table 2. Sample of WATs in ATLAS. Columns 1 and 2 give the ATLAS and SWIRE names, Column 3 gives the redshift. Column 4 lists the observed R-band magnitude from SWIRE, except for S132 where we have listed the value from super-COSMOS since a value from SWIRE is not available, while Column 5 lists the absolute R-band magnitude. Columns 6 and 7 list the flux density and luminosity respectively at 1.4 GHz. Columns 8 and 9 list the angular and physical size. All the WAT redshifts were obtained from our AAT observations with the exception of S409 whose redshift was determined by Colless et al. (2001).

ATLAS	SWIRE Counterpart	z	$R_{\rm obs}$ (mag)	$R_{\rm abs}$ (mag)	$\mathrm{Flux}_{1.4}$ (mJy)	$\mathrm{Power}_{1.4}$ (10^{24}W/Hz)	Size_{ang} (arcmin)	Size_{phys} (kpc)
ELAIS-1								
S132	SWIRE4_J003236.18-442101.1	0.3762	18.1	−23.41	5.35	2.58	1.0	309
S483	SWIRE4_J003311.21-435512.3	0.3164	18.28	−22.79	6.72	2.16	1.5	413
S1189	SWIRE4_J003427.54-430222.5	0.2193	17.12	−23.04	45.03	6.25	5.0	1053
S1192	SWIRE4_J003320.68-430203.6	0.3690	18.92	−22.54	10.46	4.82	0.9	274
CDFS								
S031	SWIRE3_J032639.11-280801.5	0.2183	16.63	−23.52	42.29	5.81	2.7	567
S409	SWIRE3_J033210.74-272635.5	0.1469	16.35	−22.84	42.35	2.41	2.6	396

finds more tailed sources at moderate and high redshifts, the opening angle of S1189 is close to that of a WAT. Although WATs do tend to be associated with the dominant galaxy, it could be associated with a bright galaxy close to the brightest galaxy in a cluster or group (see Rudnick & Owen 1977; Blanton et al. 2001). The associated galaxy of S1189 is the next brightest galaxy, only 0.75 mag fainter than the cD galaxy. Rudnick & Owen (1977) also suggested that WATs tend to have larger sizes than the narrow-angle tailed sources. With a total size of over a Mpc, it would be more consistent with the sizes of WATs. Considering all the aspects, we presently classify it as a WAT. We discuss the results of our AAOmega observations and the environment of this source in Section 4.

3.4 S1192

S1192 is similar to S132 in both shape and extent, but the two tails in S1192 are more symmetric in brightness. Both the DSS red and 3.6-μm images show a number of galaxies forming a filamentary-like structure along with the host galaxy of the WAT. The photometric redshifts (Rowan-Robinson et al. 2008) within a radius of 2 arcmin, which corresponds to $\sim$500 kpc at z=0.3690, show a concentration of galaxies at about the redshift of S1192 (Fig. 5). This overdensity is largely due to the galaxies in the filamentary-like structure.

3.5 S031

Although S031 exhibits distinct gaps of emission between the radio core and the two tails of emission, the identification process described by Norris et al. (2006) unambiguously classifies these three components as a triple radio source. The peaks of emission in the tails are towards the radio core as expected in FRI radio sources. We do not have redshift information at present to determine which of the galaxies seen in Fig. 2 may be a part of the group or cluster associated with S031. The gaps of emission between the central source and the lobes are reminiscent of the large radio galaxy in Abell 2372 (Owen & Ledlow

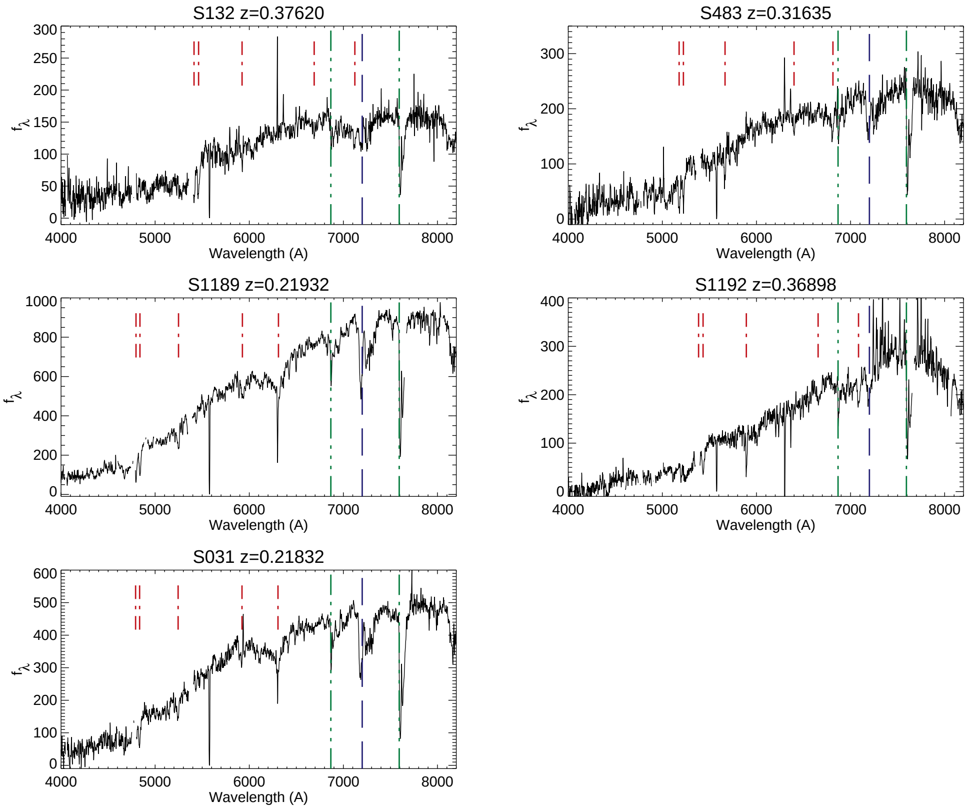

Figure 3. Spectra of the host galaxies of the five WATs for which we have measured redshifts using the AAOmega spectrograph on the AAT. The spectra are typical of early-type galaxies that host luminous radio sources. The red dot-dashed lines indicate the prominent stellar absorption features typical of an early-type galaxy spectrum (Ca H+K, G-band, H-beta and Mg-b) from which the redshift has been derived via template cross correlation. The green dash-dot-dot-dot lines indicate the Fraunhofer A+B atmospheric absorption bands from O_2 and the blue long dashed lines indicate the atmospheric water absorption band, neither of which have been corrected due to the absence of appropriate telluric standards in the redshift survey data.

1997; Giacintucci et al. 2007), which has been suggested by Giacintucci et al. (2007) to be due to recurrent radio activity (see Saikia & Jamrozy 2009 for a review). Although such a possibility cannot be ruled out, more detailed spectral and structural information are required to clarify whether this is indeed the case.

3.6 S409

S409 is the closest of the WATs in ATLAS with a redshift of 0.1469 (Colless et al. 2001) and a size of 396 kpc. It has an interesting radio structure with the western lobe exhibiting two sharp bends and forming a long narrow tail of emission. A deep X-ray image would be useful to understand how the gas distribution may have shaped the unusual radio structure. The 2dFGRS data (Colless et al. 2001) within a radius of ∼1 Mpc show a clear excess of galaxies in the same redshift bin as S409 (Fig. 6). Within a radius of 500 kpc (3.5 arcmin at z = 0.1469) we find 3 galaxies at about the redshift of S409.

4 LARGE-SCALE STRUCTURE AROUND S1189

There are a total of 309 galaxies with spectroscopic redshifts within a radius of one degree of S1189, including 94 galaxies whose redshifts we have measured from our service mode observations with the AAOmega spectrograph. The other redshifts are obtained from spectroscopic observations of ATLAS sources (Section 2.2). The redshifts of these 94 new galaxies are listed in Appendix A.

4.1 Redshift distribution

The redshifts of the 309 galaxies within a radius of one degree (∼12.6 Mpc at z ∼ 0.22) from the WAT source extend to ∼1.95. The distribution for the subset of 299 galaxies with $z \leq 0.8$ is shown in Fig. 7. The data are binned in intervals of $\Delta z = 0.005$ which corresponds to 1500 km s^{-1}. There is a clear excess of galaxies at the redshift of the WAT source, with a distinct peak at the redshift bin $0.22 \leq z < 0.225$. 20 galaxies lie in the peak-redshift bin, and a further 22 galaxies lie in the two neighbouring bins resulting in 42 galaxies over three redshift bins, the concentration being significant

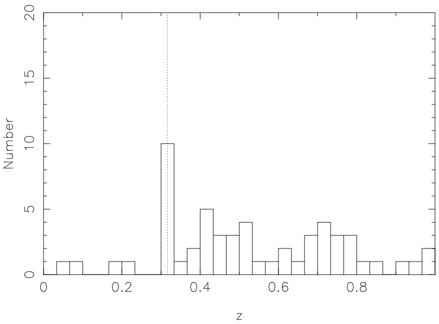

Figure 4. Photometric redshift distribution of galaxies within 2 arcmin of S483 (∼550 kpc at z = 0.3164). The data is binned in intervals of Δz = 0.03. The vertical dotted line indicates the redshift of the host galaxy.

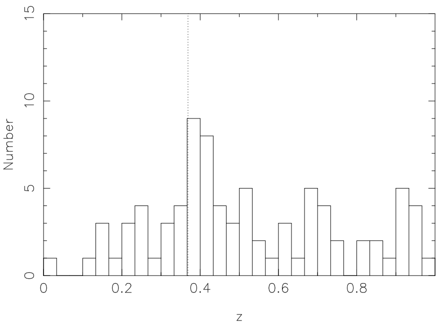

Figure 5. Photometric redshift distribution within 2 arcmin of S1192 (∼500 kpc at z = 0.3690). The data is binned in intervals of Δz = 0.03. The vertical dotted line indicates the redshift of the host galaxy.

at $\sim 7\sigma$. Properties of the galaxies in the peak histogram bin and the two adjacent bins, which includes the putative cD galaxy at a redshift of 0.2204, are listed in Table 3. The total spread in velocity of the 42 galaxies is ∼4500 km s^{-1}, and the velocity dispersion is ∼870 km s^{-1}. This is similar to the spread for typical rich clusters in the local Universe undergoing mergers such as A3667 and A3376 which both show **radio** relic emission and have a velocity spread of ∼4200 km s^{-1} (Johnston-Hollitt, Hunstead & Corbett 2008; Johnston-Hollitt et al. 2010; Owers, Couch & Nulsen 2009). The redshift distribution of the 42 galaxies is shown in greater detail as an inset in Fig. 7. The distribution is not a smooth Gaussian and shows substructure, consistent with dynamic, merging systems.

4.2 Spatial Distribution

In Fig. 8 we plot the positions of the 42 galaxies listed in Table 3, with the galaxies in the three redshift bins ($0.215 \leq z < 0.22$; $0.22 \leq z < 0.225$; $0.225 \leq z < 0.23$) indicated by circles of varying size. Despite considerable overlap, there is a suggestion of a velocity gradient with the galaxies in the lowest redshift bin (largest circles) extending towards the south-west and those in the highest redshift bin (smallest circles) extending towards the south-east. Although galaxy redshifts were measured within a radius of ∼12 Mpc from the WAT, ∼60 per cent of the galaxies listed in Table 3 are within 6 Mpc of the WAT (30 arcmin). We also note that the larger number of sources in the southern part of Fig. 8 is due to the uneven coverage of the one-degree-radius field surrounding S1189.

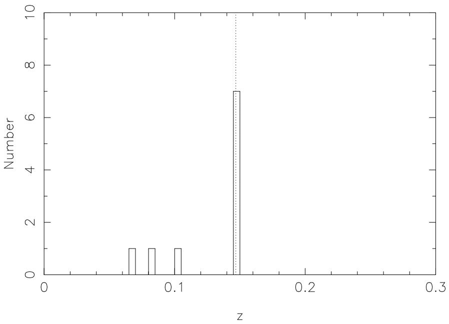

Figure 6. 2dFGRS spectroscopic redshifts (Colless et al. 2001) of sources within 7 arcmin of S409 (∼1 Mpc at z = 0.1469). The data is binned in intervals of Δz = 0.005. The vertical dotted line indicates the redshift of the host galaxy.

4.3 cD Galaxy

The bright galaxy, SWIRE3_J003419.26-430334.0, located southwest of the WAT source, has a redshift of 0.2204, implying a velocity difference between the two galaxies of ∼320 km s^{-1}. Their projected separation is ∼2 arcmin, corresponding to ∼420 kpc at a redshift of 0.22. SWIRE3_J003419.26-430334.0 is the brightest galaxy in the cluster and has a diffuse envelope, therefore we classify it as a possible cD galaxy. There is a marginal detection of associated radio emission with a flux density of ∼140 μJy at 1.4 GHz which corresponds to a radio luminosity of 1.96×10^{22} W Hz^{-1}. Centrally dominant cD galaxies are usually giant ellipticals residing in the centres of clusters of galaxies. These are much larger and brighter than other galaxies in the cluster and are often surrounded by a diffuse envelope (Matthews, Morgan & Schmidt 1964). Their large size is usually attributed to mergers and galaxy cannibalism (e.g. De Lucia & Blaizot 2007).

4.4 Extended radio sources in the vicinity of the WAT

In addition to double-lobed radio sources, radio haloes, relics and core haloes or mini haloes may also be associated with clusters of galaxies. Core-haloes are usually less than ∼500 kpc in extent and associated with the dominant galaxy in cooling core clusters. Haloes and relics are not associated with any particular galaxy, and are often larger in size. Radio haloes are usually projected towards the cluster centre, while relics are seen towards the periphery (e.g. Giovannini & Feretti 2004). There are ∼30 radio haloes in nearby (z<0.4) clusters of galaxies (e.g. Giovannini et al. 2009), and there are ∼30 clusters of galaxies with at least one radio relic (Giovannini & Feretti 2004). While models for haloes

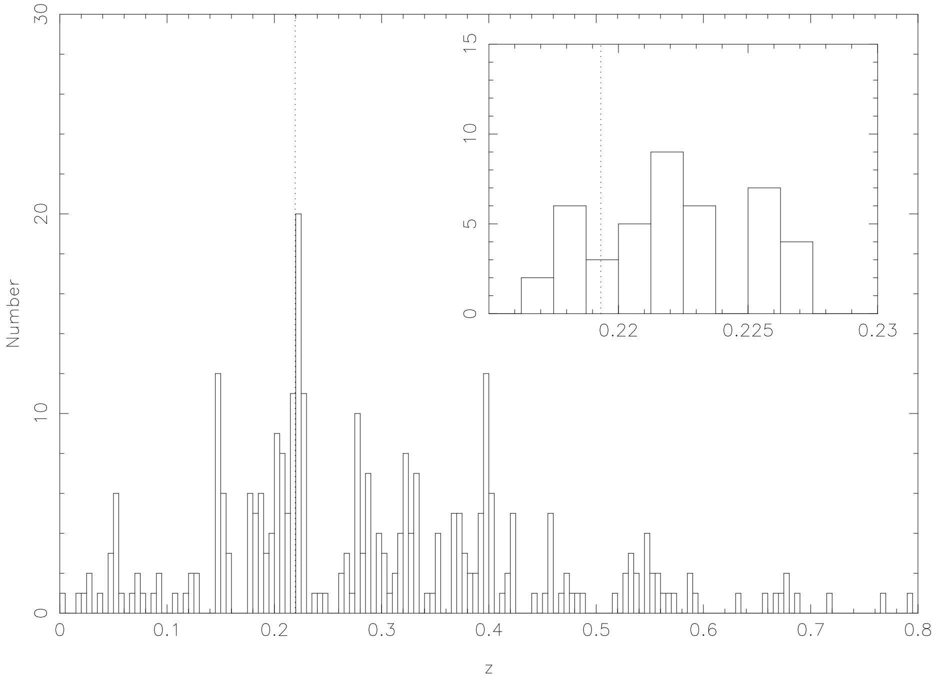

Figure 7. Histogram of redshifts of 299 galaxies located within a one degree radius centred on the WAT, S1189, and with redshifts less than or equal to 0.8. The redshift bin size is 0.005 which corresponds to 1500 km s^{-1}. The inset shows the redshift distribution of the galaxies at the peak and two adjacent bins ($0.215 \leq z < 0.23$). The redshift bin size is 0.00125 which corresponds to 375 km s^{-1}. The vertical dotted lines in both histograms are at z=0.2193, the redshift of the WAT source.

range from re-acceleration of particles by turbulence to production of relativistic electrons by hadronic collisons, relics are believed to arise due to cluster mergers and/or matter accretion (Sarazin 1999; Ryu et al. 2003; Pfrommer et al. 2006; Giacintucci et al. 2008; Johnston-Hollitt, Hunstead & Corbett 2008; Brown & Rudnick 2009).

Recent work suggests that halos are found in massive, unrelaxed clusters, with the radio and X-ray luminosity being strongly correlated, consistent with the re-acceleration scenario (Brunetti et al. 2007; Venturi et al. 2008; Cassano 2009). However, the present studies have been based on X-ray selected clusters of galaxies, and possible biases arising from it should be borne in mind. For example, the limited sensitivity of the radio observations would make it easier to detect halos in only the more X-ray luminous clusters of galaxies.

Radio relics on the other hand are believed to arise due to mergers accompanied by shocks and/or matter accretion (e.g. Bagchi et al. 2006, and references therein). These shocks are capable of accelerating particles to high energies, giving rise to the observed synchrotron radio emission. Harris, Kapahi & Ekers (1980) and Tribble (1993) were amongst the early ones to suggest and explore the possibility of acceleration of particles due to shock fronts on a large scale caused by mergers. These ideas were expanded upon by Enßlin et al. (1998), Roettiger, Burns & Stone (1999) Enßlin & Gopal-Krishna (2001) and Ricker & Sarazin (2001), producing more sophisticated models.

The ATLAS radio image at 1.4 GHz (Fig. 9) shows two more extended sources within ∼20 arcmin of the WAT source, one of which (S1081) appears to be a radio relic (Middelberg et al. 2008), while the other (S1110) is an FRI radio galaxy. Superpositions of the radio image of the relic on an optical DSS red image as well as an infrared 3.6$-\mu$m image are shown in Fig. 10. While no optical object is visible within the radio contours, there is an infrared object towards the central region of the source. This object has been classified as an Sbc galaxy (optical template type 5) using a total of 6 photometric bands by Rowan-Robinson et al. (2008). Its photometric redshift has been estimated to be 1.18. Given the properties of the object, it is likely to be unrelated. The radio properties of the WAT and these two sources are summarised in Table 4. At a redshift of 0.22, the relic would have a physical size of ∼274 kpc and a luminosity of $\mathbf{3.3}\times10^{23}$ W Hz^{-1}, which would make it similar to the relics found in the periphery of clusters of galaxies in the local Universe (Ferrari et al. 2008). The relic is at a projected distance of ∼2 Mpc from the cD galaxy. Typically relics have been observed at distances of about a Mpc from the cluster centre, although some systems are known to have relics up to distances of ∼4 Mpc (e.g. Giovannini & Feretti 2004). Some of the known examples of relics which lie at distances beyond ∼2 Mpc from the nearest cluster core, such as B0917+75 (Harris et al. 1993; Johnston-Hollitt 2003), are typically associated with structure larger than a single cluster. In the case of B0917+75 it is the Rood 27 cluster group. This is similar to

Table 3. Optical and infrared properties of the putative cluster members. Column 1 gives the SWIRE identification. Column 2 lists the R-band magnitude from SWIRE while Column 3 lists the redshifts. Column 4 lists the radio flux density at 1.4 GHz while Column 5 provides comments.

SWIRE ID	R mag	z	Radio flux (mJy)	comment
SWIRE3_J003236.91-432040.8	19.44	0.2169		
SWIRE4_J003411.57-425952.0	18.92	0.2171	0.53	
SWIRE4_J003107.43-434037.5		0.2176	0.24	
SWIRE4_J003559.43-430324.8	18.74	0.2180	0.21	
SWIRE4_J003109.85-435010.9		0.2181	3.93	
SWIRE4_J003512.31-425437.5		0.2181	14.79	
SWIRE3_J003203.05-434121.6	18.07	0.2184		
SWIRE3_J003500.92-430309.5	20.06	0.2187		
SWIRE3_J003355.92-424153.9		0.2190		
SWIRE4_J003123.87-430940.5		0.2191	0.34	
SWIRE4_J003427.54-430222.5	17.12	0.2193	45.03	WAT
SWIRE3_J003422.08-430623.7	19.53	0.2201		
SWIRE4_J003432.80-424555.1		0.2202	1.08	
SWIRE4_J003748.72-430211.9	18.65	0.2203	0.23	
SWIRE4_J003525.13-432941.4	18.93	0.2204	0.15	
SWIRE3_J003419.26-430334.0	16.37	0.2204		cD galaxy
SWIRE4_J003713.54-431342.8	17.53	0.2214	2.39	
SWIRE3_J003339.84-430908.8	18.07	0.2215		
SWIRE3_J003711.92-430711.4	18.32	0.2215		
SWIRE3_J003415.87-430840.9	18.97	0.2220		
SWIRE4_J003714.11-430833.3	17.59	0.2221	0.53	
SWIRE3_J003526.70-430418.7	18.45	0.2222		
SWIRE3_J003503.98-425710.2		0.2222		
SWIRE4_J003645.81-432016.0	17.73	0.2222	0.49	
SWIRE3_J003443.66-424544.6		0.2225		
SWIRE4_J003344.79-431627.8	17.87	0.2228	0.91	
SWIRE3_J003707.12-430302.7	19.18	0.2229		
SWIRE4_J003242.01-432630.6	18.78	0.2230	0.32	
SWIRE4_J003326.18-434051.0	18.76	0.2232	0.27	
SWIRE3_J003229.91-425457.7		0.2233		
SWIRE3_J003242.01-432630.5	18.78	0.2233		
SWIRE4_J003721.05-434240.0	17.40	0.2251	1.33	
SWIRE4_J003306.30-431029.8	17.71	0.2252	12.33	double radio
SWIRE4_J003609.95-435002.2	19.84	0.2252	0.32	
SWIRE3_J003322.00-430419.5	20.12	0.2253		
SWIRE4_J003604.09-435802.3		0.2255	0.18	
SWIRE4_J003340.23-432542.2	18.24	0.2258	0.34	
SWIRE4_J003640.42-430000.1	17.32	0.2263	0.75	
SWIRE4_J003734.09-433339.3	17.92	0.2263	1.20	
SWIRE3_J003659.30-431824.1	18.20	0.2263		
SWIRE4_J003502.52-432410.9	18.02	0.2265	0.19	
SWIRE3_J003300.09-432819.9	18.26	0.2267		

our situation. It is also relevant to note that the minor axis of the relic does not point towards either the WAT source or the cD galaxy, suggesting substructure in this large-scale structure. Simulations of shock generation during hierarchical mass assembly suggest relics can be produced over 8 Mpc from the cluster centre (Miniati et al. 2000; Pfrommer et al. 2006; Pfrommer, Enßlin & Springel 2008; Hoeft et al. 2008; Vazza, Brunetti & Gheller 2009). These aspects along with its radio structure and lack of an obvious optical identification make it very likely to be a radio relic. One could enquire whether this object might be a dying radio galaxy. The non-detection of an early-type galaxy associated with it suggests that this is unlikely to be the case. There are very few relics known beyond a redshift of ∼0.2 (e.g. Giovannini & Feretti 2004), which makes this finding a significant one.

The other interesting source in the field is the FRI radio source S1110. The radio emission from S1110 is symmetric within ∼80 kpc from the host galaxy, SWIRE4_J003306.30-431029.8, reminiscent of the large-scale jets in FRI radio sources. However, the extended lobes are highly asymmetric, the peak brightness in the outer extremities differing by a factor of ∼4. This may be due to density asymmetries on opposite sides of the source.

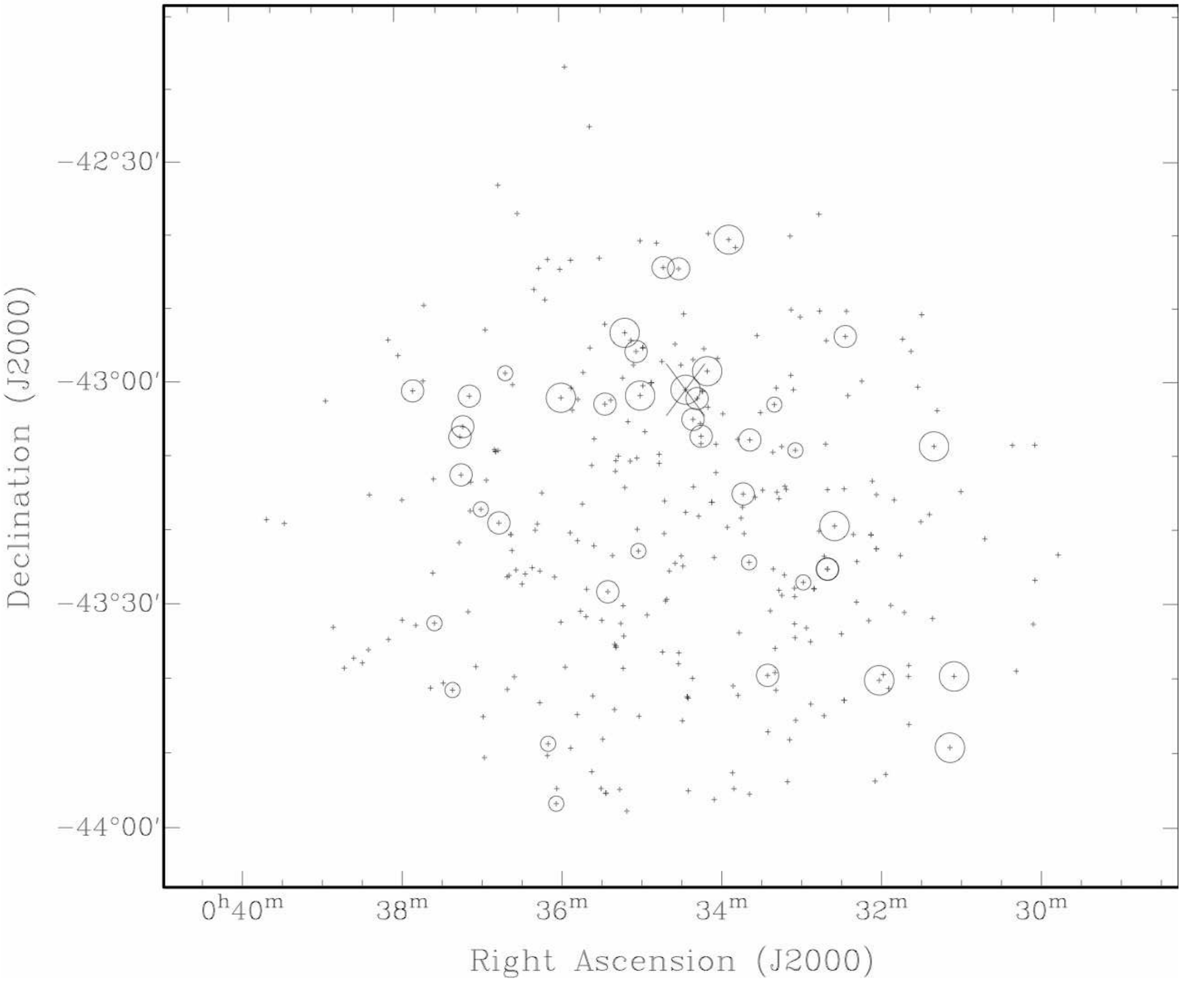

Figure 8. Spatial distribution of all galaxies in the field surrounding S1189 that have spectroscopic redshifts. The circled sources are at $0.215 \leq z < 0.23$. The largest circles show the sources that are at $0.215 \leq z < 0.22$. The medium circles show the sources that are at $0.22 \leq z < 0.225$ and the smallest circles show the sources that are at $0.225 \leq z < 0.23$. The location of the WAT is indicated by the large "X".

Table 4. Radio properties of S1189 and extended radio sources in its vicinity. The size of the WAT (S1189) was measured from the outer edge of one lobe to the core and out to the outer edge of the other lobe. The relic is assumed to be at a redshift of 0.22.

	ATLAS ID	RA (J2000)	Dec (J2000)	Redshift	$S_{1.4}$ (mJy)	$\mathrm{Power}_{1.4}$ (10^{24} W Hz^{-1})	size_{ang} (arcmin)	size_{phy} (kpc)
WAT	S1189	00 34 27.6	-43 02 22.5	0.2193	45.03	6.25	5.0	1053
Double radio	S1110	00 33 06.3	-43 10 29.8	0.2252	12.33	1.82	2.6	559
Relic	S1081	00 34 11.7	-43 12 39.4	(0.22)	2.35	(0.33)	1.25	(274)

5 IMPLICATIONS FOR DEEP WIDE RADIO SURVEYS AND ATLAS

In this paper we have reported the detection of six WATs from a sample of 2004 radio sources. Extrapolating this to future deep wide surveys, we might expect to detect about 200,000 WATs from the catalogue of 70 million radio sources that will be generated by the ASKAP-EMU (Australia SKA Pathfinder - Evolutionary Map of the Universe) project (Norris et al. 2009). Since each of these WATs is likely to be associated with a cluster, such surveys will be powerful tools for detecting clusters and exploring their properties, particularly since the radio luminosity of WATs makes them detectable and capable of being studied up to high redshifts.

Such surveys are therefore likely to contribute significantly to areas such as the formation and evolution of clusters, the formation of massive ellipticals,

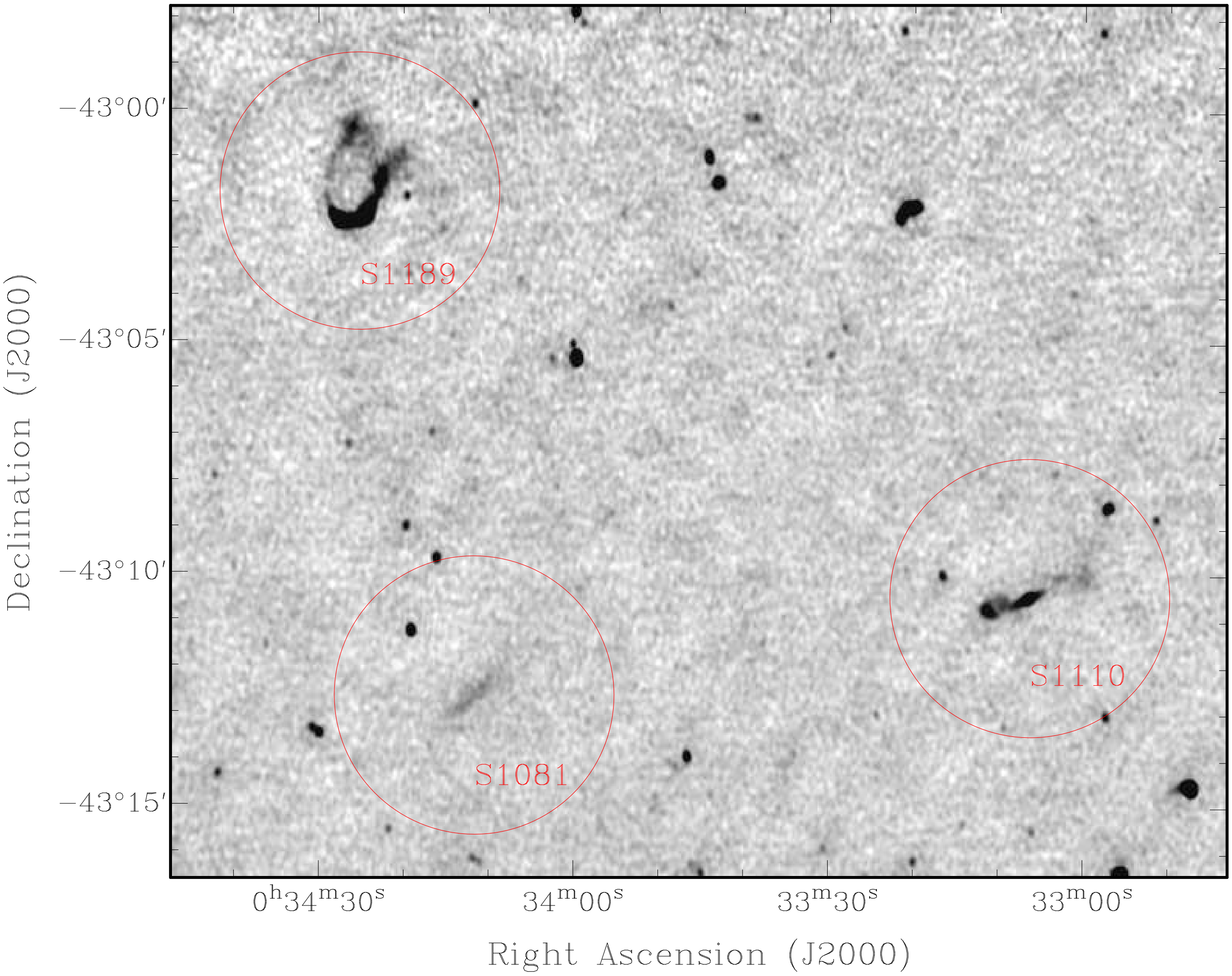

Figure 9. 1.4 GHz radio image showing the WAT (S1189), the double-lobed radio galaxy (S1110) and the radio relic (S1081). The WAT S1192 , at z = 0.3690, is also seen in the image.

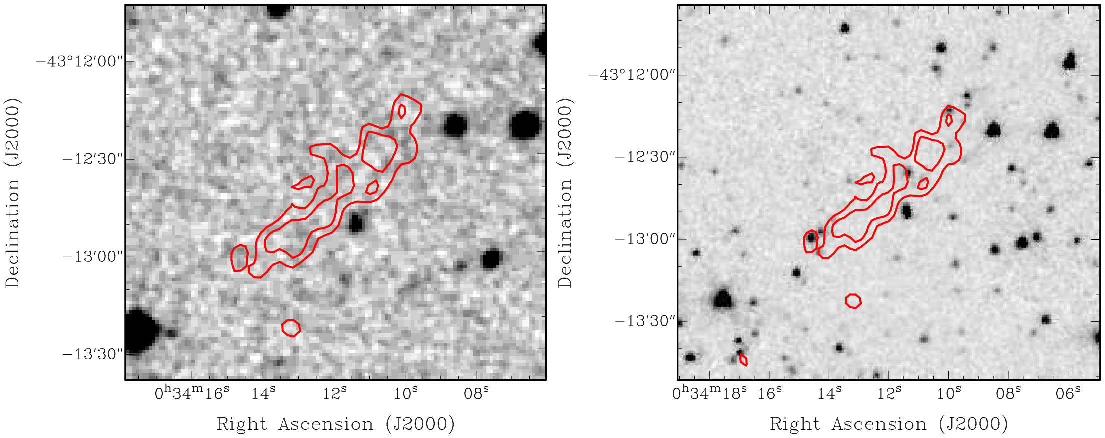

Figure 10. 1.4 GHz radio contours of the relic (S1081) overlaid on the DSS red optical image (left panel) and the 3.6 μm IRAC image (right panel) The contours start at 100 μJy beam^{-1} and increase by factors of $\sqrt{2}$.

and the relationship between giant ellipticals and supermassive black holes, or SMBHs (e.g. Blanton et al. 2003; Chiaberge et al. 2009). Furthermore, while optical and X-ray surveys tend to select the optically-rich or most X-ray-luminous clusters of galaxies at moderate and high redshifts, sensitive radio observations could help identify clusters with a wide range of optical and X-ray properties.

However, WATs are characterized by diffuse lobes of emission extending to hundreds of kpc, and two effects potentially make such structures difficult to observe at high redshift.

First, the radiating electrons of a synchrotron source lose energy by inverse-Compton (iC) scattering of the cosmic microwave background radiation (CMBR), whose energy density increases as $(1+z)^4$. This effect is supported by evidence that the X-ray emission from the lobes of large radio galaxies is due to iC scattering of the radiating electrons with the CMBR, which has been used to make an independent estimate of the magnetic field strength of the radio lobes (e.g. Croston et al. 2004, 2005; Konar et al. 2009). Furthermore, Konar et al. (2004) have found that the bridge emission in giant radio sources is less prominent at higher redshifts, which they interpret as being caused by iC scattering with the CMBR.

Loss of electron energy by iC scattering from the CMBR overtakes synchrotron cooling at a redshift $z \sim 0.556\sqrt{B} - 1$ where B is the synchrotron magnetic flux density in μGauss (Schwartz et al. 2006). So, for a constant B, one might expect synchrotron emission to fall sharply above that redshift.

However, if a low-luminosity radio source is modelled as two cones of expanding plasma on either side of the central SMBH, then the magnetic field would be expected to fall as the square of the distance r from the SMBH, resulting in a transition radius r_{crit} at which the dominant electron cooling mechanism switches from synchrotron to iC, where $r_{crit} \propto (1+z)^{-1}$. Thus, rather than synchrotron emission falling sharply above some redshift, the size of the synchrotron-emitting region shrinks linearly with redshift.

We conclude that, while iC cooling reduces the apparent size of the emitting region, it does not impose a fundamental redshift limit above which WATs will be invisible.

Second, high-redshift galaxies are subject to cosmological surface brightness dimming, (e.g. Lanzetta et al. 2002, and references therein) which causes the observed surface brightness per unit frequency interval of a resolved source to decrease as $(1+z)^3$. Thus, nearby radio galaxies are detectable to much lower intrinsic surface brightness thresholds than high-redshift sources.

While both these effects are going to present challenges to the identification of WATs at high redshifts, they accentuate the normal challenges of resolution and sensitivity, rather than presenting fundamental limits of observability. In their search for FRI radio sources in the redshift range $1<z<2$ using the Faint Images of the Radio Sky at Twenty-Centimeters (FIRST) radio survey, Chiaberge et al. (2009) find that most of the sources are compact. Blanton et al. (2003) have identified a WAT galaxy at z=0.96, while Saikia, Wiita & Muxlow (1993) and Saikia et al. (1987) explored the possibility that B1222+216 (4C21.35) and B2 1419+315 might be WAT quasars at redshifts of 0.435 and 1.547 respectively.

To explore and understand these aspects will require more detailed modelling and significantly deeper large-scale radio surveys, which is the primary goal of ASKAP-EMU.

6 CONCLUSIONS

We have identified a sample of six Wide-Angle Tail (WAT) radio sources. We present new spectroscopic redshifts for four of these sources, and find that these WATs lie in the redshift range 0.1469−0.3762. We have examined the fields using both spectroscopic and photometric redshifts of galaxies in the vicinity of the WATs and find evidence of an overdensity of galaxies in four of these WATs.

From a more detailed study of the field around S1189 we find an overdensity of galaxies which is spread over ∼12 Mpc and has a velocity spread of ∼4500 km s^{-1}, and a velocity dispersion of ∼870 km s^{-1}. This large-scale structure hosts a putative cD galaxy with, at best, weak radio emission, a radio relic which has a size of ∼274 kpc, and an asymmetric FRI radio galaxy with an extent of ∼559 kpc. The peak brightness at the extremities of the outer lobes of the FRI source differ by a factor of ∼4, possibly due to differences in the environment on opposite sides. The minor axis of the relic is not directed towards either the host galaxy of the WAT or the putative cD galaxy. This large-scale structure may represent an unrelaxed system with different sub-structures interacting or merging with one another. Therefore, deep X-ray observations of the field would be very valuable to further understand this interesting large-scale structure.

WATs are known to occur in clusters of galaxies, and could in principle be useful tracers of clusters at moderate and high redshifts. IC cooling of electrons by interaction with CMBR increases rapidly with z. However, this does not imply a sharp drop in the number of WATs at high z. Deep and wide-field surveys, such as the Evolutionary Map of the Universe (EMU) (Norris et al. 2009), should provide additional information and insights on the range of structures at moderate and high redshifts. We expect these to be invaluable probes of large-scale structure.

ACKNOWLEDGEMENTS

We thank Emil Lenc and Jamie Stevens for their help, the ATLAS team and Mark Birkinshaw for many fruitful discussions, and an anonymous referee whose comments helped improve the manuscript. MYM acknowledges the support of an Australian Postgraduate Award as well as Postgraduate Scholarships from AAO and ATNF. We thank the staff at AAO and ATCA for making these observations possible. The ATCA is part of the Australia Telescope, which is funded by the Commonwealth of Australia for operation as a National Facility managed by CSIRO. This research has also made use of NASA's Astrophysics Data System.

REFERENCES

Bagchi J., Durret F., Neto G. B. L., Paul S., 2006, Sci, 314, 791

Blanton E. L., Gregg M. D., Helfand D. J., Becker R. H., White R. L., 2000, ApJ, 531, 118

Blanton E. L., Gregg M. D., Helfand D. J., Becker R. H., Leighly K. M., 2001, AJ, 121, 2915

Blanton E. L., Gregg M. D., Helfand D. J., Becker R. H., White R. L., 2003, AJ, 125, 1635

Böhringer H., et al., 2001, A&A, 369, 826

Borgani S., et al., 2004, MNRAS, 348, 1078

Brown S., Rudnick L., 2009, AJ, 137, 3158

Brunetti G., Venturi T., Dallacasa D., Cassano R., Dolag K., Giacintucci S., Setti G., 2007, ApJ, 670, L5

Burns J. O., 1990, AJ, 99, 14

Burns J. O., 1998, Science, 280, 400

Cassano R., 2009, in The Low-Frequency Radio Universe, eds Saikia D.J., Green D.A., Gupta Y, Venturi T., ASPC, 407, 223

Chiaberge M., Tremblay G., Capetti A., Macchetto F. D., Tozzi P., Sparks W. B., 2009, ApJ, 696, 1103

Colless M., et al., 2001, MNRAS, 328, 1039

Croston J. H., Birkinshaw M., Hardcastle M. J., Worrall D. M., 2004, MNRAS, 353, 879

Croston J. H., Hardcastle M. J., Harris D. E., Belsole E., Birkinshaw M., Worrall D. M., 2005, ApJ, 626, 733

De Lucia G., Blaizot J., 2007, MNRAS, 375, 2

Enßlin T. A., Biermann P. L., Klein U., Kohle S., 1998, A&A, 332, 395

Enßlin T. A., Gopal-Krishna, 2001, 366, 26

Fanaroff B. L., Riley J. M., 1974, MNRAS, 167, 31P

Feretti L., 2005, AdSpR, 36, 729

Ferrari C., Govoni F., Schindler S., Bykov A. M., Rephaeli Y., 2008, SSRv, 134, 93

Giacintucci S., Venturi T., 2009, A&A, 505, 55

Giacintucci S., Venturi T., Murgia M., Dallacasa D., Athreya R., Bardelli S., Mazzotta P., Saikia D.J., 2007, A&A, 476, 99

Giacintucci S., et al., 2008, A&A, 486, 347

Giovannini G., Feretti L., 2000, NewA, 5, 335

Giovannini G., Feretti L., 2004, JKAS, 37, 323

Giovannini G., Bonafede A., Feretti L., Govoni F., Murgia M., Ferrari F., Monti G., 2009, A&A, 507, 1257

Harris D.E., Kapahi V.K., Ekers R.D., 1980, A&AS, 39, 215

Harris D. E., Stern C. P., Willis A. G., Dewdney P. E., 1993, AJ, 105, 769

Hoeft M., Brüggen M., Yepes G., Gottlöber S., Schwope A., 2008, MNRAS, 391, 1511

Johnston-Hollitt M., 2003, PhD Thesis, University of Adelaide

Johnston-Hollitt M., Hunstead R. W., Corbett E., 2008, A&A, 479, 1

Johnston-Hollitt M., Gill J. A., Hollitt C. P., Tunstall L. 2010, MNRAS, submitted

Kantharia N.G., Das M., Gopal-Krishna, 2009, JApA, 30, 37

Konar C., Saikia D. J., Ishwara-Chandra C. H., Kulkarni V. K., 2004, MNRAS, 355, 845

Konar C., Hardcastle M. J., Croston J. H., Saikia D. J., 2009, MNRAS, 400, 480

Kravtsov A., et al., 2009, astro, 2010, 164

Lanzetta K. M., Yahata N., Pascarelle S., Chen H.-W., Fernández-Soto A., 2002, ApJ, 570, 492

Lewis I. J., et al., 2002, MNRAS, 333, 279

Lonsdale C. J., et al., 2003, PASP, 115, 897

Mao M. Y., Johnston-Hollitt M., Stevens J. B., Wotherspoon S. J., 2009a, MNRAS, 392, 1070

Mao M. Y., Norris R. P., Sharp R., Lovell J. E. J., 2009b, ASPC, 408, 380

Matthews T. A., Morgan W. W., Schmidt M., 1964, ApJ, 140, 35

Middelberg E., et al., 2008, AJ, 135, 1276

Miniati F., Ryu D., Kang H., Jones T. W., Cen R., Ostriker J. P., 2000, ApJ, 542, 608

Miszalski B., Shortridge K., Saunders W., Parker Q. A., Croom S. M., 2006, MNRAS, 371, 1537

Norris R. P., et al., 2006, AJ, 132, 2409

Norris R. P., the EMU team, 2009, PoS(PRA2009) 033

Oklopčić A., et al., 2010, ApJ, 713, 484

Owen F. N., Rudnick L., 1976, ApJ, 205, L1

Owen F. N., Ledlow M. J., 1994, ASPC, 54, 319

Owen F. N., Ledlow M. J., 1997, ApJS, 108, 41

Owers M. S., Couch W. J., Nulsen P. E. J., 2009, ApJ, 693, 901

Pfrommer C., Springel V., Enßlin T. A., Jubelgas M., 2006, MNRAS, 367, 113

Pfrommer C., Enßlin T. A., Springel V., 2008, MNRAS, 385, 1211

Pinkney J., Burns J. O., Ledlow M. J., Gómez P. L., Hill J. M., 2000, AJ, 120, 2269

Pratt G. W., Croston J. H., Arnaud M., Böhringer H., 2009, A&A, 498, 361

Ricker P. M., Sarazin C. L., 2001, ApJ, 561, 621

Roettiger K., Burns J.O., Stone J.M., 1999, ApJ, 518, 603

Rowan-Robinson, M., et al. 2008, MNRAS, 386, 697

Rudnick L., Owen F.N., 1977, AJ, 82, 1

Ryu D., Kang H., Hallman E., Jones T. W., 2003, ApJ, 593, 599

Sahlén M., et al., 2009, MNRAS, 397, 577

Saikia D. J., Jamrozy M., 2009, BASI, 37, 63 (arXiv:1002.1841)

Saikia D. J., Wiita P. J., Muxlow T. W. B., 1993, AJ, 105, 1658

Saikia D. J., Staveley-Smith L., Wills D., Cornwell T. J., Salter C. J., Junor W., Shastri P., 1987, MNRAS, 229, 495

Sarazin C. L., 1999, ApJ, 520, 529
Saunders W., et al., 2004, SPIE, 5492, 389
Schwartz D. A., et al., 2006, ApJ, 640, 592
Sharp R., et al., 2006, SPIE, 6269, 14
Smolcić V., et al., 2007, ApJS, 172, 295
Tribble P. C., 1993, MNRAS, 263, 31
Vazza F., Brunetti G., Gheller C., 2009, MNRAS, 395, 1333
Venturi T., Giacintucci S., Dallacasa D., Cassano R., Brunetti G., Bardelli S., Setti G., 2008, A&A, 484, 327
Wright E. L., 2006, PASP, 118, 1711

APPENDIX A: NEW REDSHIFTS

Table A1. New redshifts of galaxies near S1189.

SWIRE ID	z	SWIRE ID	z
SWIRE3_J003134.02-425148.8	0.21061	SWIRE3_J003443.66-424544.6	0.22247
SWIRE3_J003147.97-432431.8	0.44433	SWIRE3_J003445.06-425832.2	0.42247
SWIRE3_J003152.98-431701.7	0.24509	SWIRE3_J003446.92-431108.0	0.32148
SWIRE3_J003203.05-434121.6	0.21837	SWIRE3_J003446.92-431221.4	0.02507
SWIRE3_J003205.98-432339.9	0.39604	SWIRE3_J003448.84-424223.5	0.38740
SWIRE3_J003209.95-432147.1	0.20451	SWIRE3_J003452.68-430124.9	0.18383
SWIRE3_J003223.48-432147.1	0.27936	SWIRE3_J003455.92-433249.9	0.18833
SWIRE3_J003229.13-434406.2	0.35209	SWIRE3_J003458.93-430150.5	0.31710
SWIRE3_J003229.91-425457.7	0.22330	SWIRE3_J003458.95-425637.6	0.32933
SWIRE3_J003236.91-432040.8	0.21686	SWIRE3_J003459.03-425642.3	0.33043
SWIRE3_J003242.01-432630.5	0.22334	SWIRE3_J003500.92-430309.5	0.21871
SWIRE3_J003243.83-430936.9	0.20711	SWIRE3_J003501.04-424205.0	0.41316
SWIRE3_J003243.91-425533.9	0.14944	SWIRE3_J003503.98-425710.2	0.22218
SWIRE3_J003248.95-425132.5	0.21149	SWIRE3_J003506.23-425900.7	0.12141
SWIRE3_J003249.79-423818.9	0.30177	SWIRE3_J003509.89-430642.4	0.20673
SWIRE3_J003251.92-432910.4	0.28767	SWIRE3_J003513.81-430046.2	0.32167
SWIRE3_J003300.09-432819.9	0.22674	SWIRE3_J003519.09-431158.8	0.17832
SWIRE3_J003308.14-430217.3	0.18372	SWIRE3_J003526.70-430418.7	0.22216
SWIRE3_J003309.95-430020.2	0.37209	SWIRE3_J003526.75-435641.2	0.32339
SWIRE3_J003310.94-424121.5	1.24725	SWIRE3_J003527.25-425327.0	0.04506
SWIRE3_J003312.88-431547.4	0.27951	SWIRE3_J003530.92-424426.3	0.53011
SWIRE3_J003313.91-432722.2	0.33233	SWIRE3_J003535.18-430900.6	0.32241
SWIRE3_J003317.94-432925.6	0.19152	SWIRE3_J003537.70-422625.0	0.03611
SWIRE3_J003322.00-430419.5	0.22525	SWIRE3_J003538.08-425640.0	0.26549
SWIRE3_J003322.79-431047.0	0.07282	SWIRE3_J003542.74-425959.5	0.05296
SWIRE3_J003335.04-425458.6	0.21277	SWIRE3_J003551.83-424442.1	0.07070
SWIRE3_J003339.84-430908.8	0.22149	SWIRE3_J003552.04-430205.0	0.18486
SWIRE3_J003343.91-432149.5	0.40215	SWIRE3_J003552.98-432142.4	0.39342
SWIRE3_J003348.84-430904.4	0.20033	SWIRE3_J003556.02-421810.9	0.24246
SWIRE3_J003351.10-424258.2	0.26489	SWIRE3_J003556.95-433947.0	0.42403
SWIRE3_J003355.92-424153.9	0.21902	SWIRE3_J003600.06-424555.6	0.54820
SWIRE3_J003400.08-430537.8	0.20725	SWIRE3_J003609.00-424433.8	0.18637
SWIRE3_J003403.95-425805.9	0.32737	SWIRE3_J003611.10-425004.1	0.33055
SWIRE3_J003404.81-431335.8	0.18986	SWIRE3_J003619.16-424839.2	0.20139
SWIRE3_J003404.90-430945.6	0.27894	SWIRE3_J003630.77-423814.6	0.05462
SWIRE3_J003408.19-431736.3	0.14801	SWIRE3_J003636.80-432152.6	0.15536
SWIRE3_J003410.81-424105.3	0.27872	SWIRE3_J003645.06-423419.9	0.32288
SWIRE3_J003410.96-430444.7	0.42139	SWIRE3_J003645.88-431028.3	0.30023
SWIRE3_J003413.83-425647.6	0.32816	SWIRE3_J003647.94-431037.1	0.29938
SWIRE3_J003415.22-430234.2	0.18821	SWIRE3_J003655.07-425404.1	0.27827
SWIRE3_J003415.87-430840.9	0.22201	SWIRE3_J003659.30-431824.1	0.22634
SWIRE3_J003419.26-430334.0	0.22040	SWIRE4_J003706.38-431442.3	0.66842
SWIRE3_J003421.99-425817.0	0.41943	SWIRE3_J003706.70-431836.0	0.01959
SWIRE3_J003422.08-430623.7	0.22014	SWIRE3_J003707.12-430302.7	0.22293
SWIRE3_J003426.01-434349.1	0.20469	SWIRE3_J003711.92-430711.4	0.22153
SWIRE3_J003428.82-425203.7	0.12161	SWIRE3_J003728.02-434143.2	0.20727
SWIRE3_J003430.97-425901.6	0.14762	SWIRE3_J003748.09-433353.8	0.30986